SCIENCE CHINA
Technological Sciences

Special Topic: High-speed Railway Infrastructure
• Article •

October 2014 Vol.57 No.10: 1883–1894
doi: 10.1007/s11431-014-5636-8

Damage evolution and dynamic response of cement asphalt mortar layer of slab track under vehicle dynamic load

ZHU ShengYang[1], FU Qiang[2], CAI ChengBiao[1*] & SPANOS Pol D[3]

[1] *State Key Laboratory of Traction Power, Southwest Jiaotong University, Chengdu 610031, China;*
[2] *School of Civil Engineering, Central South University, Changsha 410075, China;*
[3] *Ryon Chair in Engineering, Rice University, Houston 77005, USA*

Received March 28, 2014; accepted June 23, 2014

The damage evolution and dynamic performance of a cement asphalt (CA) mortar layer of slab track subjected to vehicle dynamic load is investigated in this paper. Initially, a statistical damage constitutive model for the CA mortar layer is developed using continuous damage mechanics and probability theory. In this model, the strength of the CA mortar elements is treated as a random variable, which follows the Weibull distribution. The inclusion of strain rate dependence affords considering its influence on the damage development and the transition between viscosity and elasticity. Comparisons with experimental data support the reliability of the model. A three-dimensional finite element (FE) model of a slab track is then created with the commercial software ABAQUS, where the devised model for the CA mortar is implemented as a user-defined material subroutine. Finally, a vertical vehicle model is coupled with the FE model of the slab track, through the wheel-rail contact forces, based on the nonlinear Hertzian contact theory. The evolution of the damage and of the dynamic performance of the CA mortar layer with various initial damage is investigated under the train and track interaction. The analysis indicates that the proposed model is capable of predicting the damage evolution of the CA mortar layer exposed to vehicle dynamic load. The dynamic compressive strain, the strain rate, and the induced damage increase significantly with an increase in the initial damage, whereas the dynamic compressive stress exhibits a sharp decrease with the increasing initial damage. Also, it is found that the strain rate dependence significantly influences the damage evolution and the dynamic behavior of the CA mortar layer.

cement asphalt mortar, slab track, statistical damage constitutive model, vehicle-track coupled dynamics, damage evolution

Citation: Zhu S Y, Fu Q, Cai C B, et al. Damage evolution and dynamic response of cement asphalt mortar layer of slab track under vehicle dynamic load. Sci China Tech Sci, 2014, 57: 1883–1894, doi: 10.1007/s11431-014-5636-8

1 Introduction

High-speed railway lines in the form of slab tracks in Europe, China and Japan have been widely constructed. This is because of the fact that this construction offers better stiffness uniformity, higher running stability, and lower maintenance cost [1–3]. In the slab tracks, the CA mortar layer is placed between the slab and the concrete base to ensure desirable elevation and high smoothness of the slab tracks. It is critical as it not only enhances the structural integrity through its bonding constraints to the slab and the concrete base, but also improves the riding comfort of high-speed vehicles by absorbing a certain amount of vibrations.

Although the slab tracks have experienced improvements in their applications in high-speed railway lines compared with traditional ballasted tracks, the slab tracks still exhibit certain disadvantages. Premature structural damage has occurred in nearly all kinds of the slab tracks caused by a variety of factors. On the Chinese high-speed railway lines, the damage or deterioration of the CA mortar layer are rec-

*Corresponding author (email: cbcai@home.swjtu.edu.cn)

ognized as one of the most critical issues after a short-time operation, as shown in Figure 1. Such damage modes not only increase the cost of railway operation, but also significantly weaken the structural integrity of the slab track system, and contribute to the potential for failure of the slab tracks.

The CA mortar layers could have damaged from the construction site itself by certain construction processes such as grouting. During the service life of the CA mortar layers, the damage or cracks could also be introduced into them by several mechanisms. These include the vehicle dynamic loads because of the wheel-rail interactions, the thermal expansion mismatch between the different materials of the slab track system, and the temperature gradient load induced by temperature change. The vehicle dynamic load is one of the most dominant causes for this premature degradation of the CA mortar layers in the slab track system. Although good quality control mechanisms and quality assurance could eliminate the initial damage of pre-service CA mortar layers, the CA mortar layers in operations may not be completely defect-free. Although collapsing of railway track structures as a direct result of the damage of the CA mortar layers has rarely been reported, maintenance of these deteriorated components has been a heavy burden on the modern railway networks. Therefore, a fundamental understanding of the damage development mechanisms and the dynamic performance for the CA mortar layer is quite desirable. However, quite a few studies with regard to these research topics have been published. Xie et al. [5] studied the uniaxial compressive characteristics of the CA mortar specimens under different strain rates, revealing that the compressive strength, the maximum strain and the elastic modulus are all dependent on the strain rate. Zeng et al. [6] tested the accelerations of the CA mortar samples as well as regular concrete samples under impact loads, showing that the CA mortar material has better performance for vibration isolations compared with the regular concrete. Zhu and Cai [7] introduced a cohesive zone model with a non-linear constitutive law to model the interface damage between the CA mortar layer and the track slab. They investigated the interface damage evolution under the joint action of temperature change and vehicle dynamic loads derived by the vehicle–track coupled dynamic model. Liu and Zhao [8] analyzed the warping deformation and the stress of the slab tracks under the action of the measured temperature gradient. They found that the emergence of the interface damage between the CA mortar layers and the slabs could be caused by the alternative variations of the warping compressive and the tensile stresses. Shao et al. [9] studied the effect of temperature variation on the interface crack between the track slab and the CA mortar layer, by measuring 24 track slabs in straight sections and curve sections of the Harbin-Dalian high-speed railway without laying the CRTS I track slab. Nevertheless, modeling the degradation in the mechanical properties of the CA mortar layers under vehicle dynamic load is yet an essential challenging task for railway engineering researchers. The damage mechanism and the dynamic behavior of the CA mortar layers is rarely ascertained. This is because of the complexity of the constitutive modeling of its distinctive behavior, particularly if three-dimensional dynamic analyses must be conducted. Some attention must then be devoted to the development of an appropriate constitutive model adequate for the intended analysis of the CA mortar layers with reasonable computational efforts.

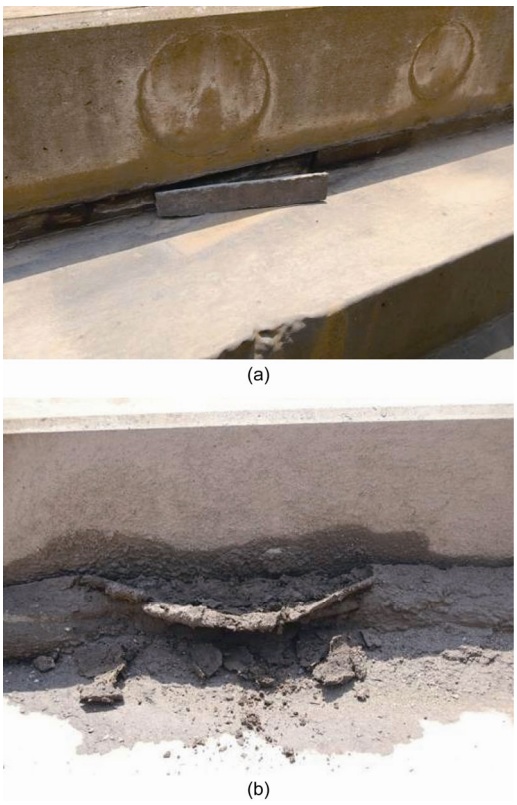

Figure 1 (Color online) Premature damage of the CA mortar layer [4]. (a) In the CRTS II slab track system; (b) in the CRTS I slab track system.

This paper presents a statistical damage constitutive model for the CA mortar layer that considers the strain rate dependence. It is implemented in the dynamic analysis of coupled vehicle-slab track systems. Also, a three-dimensional finite element (FE) model of a slab track is established coupled with a vehicle model through the wheel-rail contact forces, based on the nonlinear contact theory. The aim of the present work is to investigate the damage evolution and the dynamic performance of the CA mortar layer of the slab track subjected to vehicle dynamic load. The rest of this paper is organized as follows. Section 2 outlines the derivation of the statistical damage constitutive model for the CA mortar, where a brief description of the constitutive law, the definition of the volume element strength, and the parameters determination of the model are presented. Section 3 shows the establishment of the coupled vehicle-slab track dynamic model. This includes a brief description of the vehicle dynamic model, and the three-dimensional FE model of the slab track implemented with the presented

constitutive model for the CA mortar layer. Section 4 discusses the results which involve the experimental validation of the constitutive model, the inclusion of the strain rate dependence in the model, the evolutions of the damage, and the dynamic performance of the CA mortar layer of the slab track subjected to the vehicle dynamic load. The numerical results obtained may prove useful in the design and maintenance of the CA mortar layer of the railway slab tracks .

2 Statistical damage constitutive model for the CA mortar

2.1 Constitutive law of the model

As it is widely recognized continuum damage mechanics (CDM) is a combination of the internal state variable theory and the thermodynamics of irreversible processes. It provides a powerful framework for the derivation of consistent constitutive models suitable for a wide range of engineering problems [10–17]. This approach is appealling because it involves a computationally efficient technique and has the intrinsic simplicity and versatility of the approach, as well as its consistency. The CDM is based on the definition of the effective stress concept, which is introduced in connection with the hypothesis of strain equivalence [10,11]: The strain associated with a damaged state under the nominal stress σ is equivalent to the strain associated with its undamaged state under the effective stress $\boldsymbol{\sigma}^*$. In the present work, the effective stress tensor $\boldsymbol{\sigma}^*$ of the CA mortar will be expressed in the form

$$\boldsymbol{\sigma} = \boldsymbol{\sigma}^*(1-D) = (1-D)\boldsymbol{H}\boldsymbol{\varepsilon}, \tag{1}$$

where D denotes a scalar describing the amount of isotropic damage. This damage variable evolves between "zero" at the original elastic stage up to "one" at the material failure, and at any instant it quantifies the deterioration at a given point. The symbol $\boldsymbol{H}$ is the elastic stiffness matrix of the undamaged material and $\boldsymbol{\varepsilon}$ is the total strain matrix.

Consider the CA mortar layer as a collection of a number of small volume elements. Then, the scalar damage variable D is defined as the density of the damaged volume elements N' with respect to the total volume elements N, expressed as

$$D = \frac{N'}{N}. \tag{2}$$

As described previously, there might be many pre-service defects included in the CA mortar material, which make its mechanical properties exhibit great uncertainty and randomness. Hence, the strength of the volume elements F^* here is regarded as a random variable, which is assumed to follow the Weibull distribution, and its probability density function can be determined by the equation

$$P[F^*] = \frac{m}{F_0}\left(\frac{F^*}{F_0}\right)^{m-1}\exp\left[-\left(\frac{F^*}{F_0}\right)^m\right], \tag{3}$$

where m and F_0 are the variables involved in the Weibull distribution.

When the stress of the volume elements reaches a certain level, the number of the damaged volume elements can be obtained as

$$N' = N\int_0^{F^*} P[F^*]dF^* = N\int_0^{F^*}\frac{m}{F_0}\left(\frac{F^*}{F_0}\right)^{m-1}\exp\left[-\left(\frac{F^*}{F_0}\right)^m\right]dF^*$$
$$= N\left\{1-\exp\left[-\left(\frac{F^*}{F_0}\right)^m\right]\right\}. \tag{4}$$

By substituting eq. (4) into eq. (2), the damage variable is derived as

$$D = \frac{N\left\{1-\exp\left[-\left(\frac{F^*}{F_0}\right)^m\right]\right\}}{N} = 1-\exp\left[-\left(\frac{F^*}{F_0}\right)^m\right]. \tag{5}$$

In this work, the damage and the failure of the CA mortar are considered as a continuum process, and are based on the following assumptions. 1) The macroscopic behavior of the CA mortar is isotropic, and the damage evolves equally in all directions. 2) The CA mortar material is linearly elastic before its failure.

Using eqs. (1) and (5), the statistical damage constitutive model for the CA mortar in terms of the nominal stress are introduced as

$$\sigma_i = E\varepsilon_i(1-D) + \mu\left(\sigma_j+\sigma_k\right)$$
$$= E\varepsilon_i\exp\left[-\left(\frac{F^*}{F_0}\right)^m\right] + \mu\left(\sigma_j+\sigma_k\right), \tag{6}$$

where i=1, 2, 3, j=1, 2, 3, k=1, 2, 3, and $i \neq j \neq k$. The symbols E and u are the Young's modulus and Poisson ratio, respectively. Note that eq. (6) characterizes the full stress tensor, and therefore, the model is not only devised to predict the failures under the uniaxial loading, but it can also deal with the failures because of the complicated loading conditions.

2.2 Definition of volume element strength

The selection of the strength criterion for the volume element of the CA mortar relates primarily to the difference in the mechanical behavior of the CA mortar compared with other materials. The Mohr-Coulomb [18,19] and Drucker-Prager [20–22] criterions, commonly used in the geotechnical materials, are based on the cohesive strength and the internal friction angle. Therefore, they are only suitable for the mechanical analysis of elastic-plastic materials. Constitutive models encountered in literature based on the Hook-Brown criterion that account for the stress Lode angle are

usually characterized by many parameters, thereby making it difficult to handle in engineering applications. However, the CA mortar is a typical viscoelastic material, which exhibits the ductile failure mode, as shown in Figure 2. To account for this requisite, the Mises strength criterion, widely used to investigate the mechanical properties of ductile metal materials, is adopted here for the volume element of the CA mortar. In this criterion, the equivalent stress is taken as the research object, which has a constant value under a plastic state, and it is only dependent on material deformations. This stress is

$$F^* = \frac{1}{\sqrt{2}}\sqrt{\left(\sigma_1^* - \sigma_2^*\right)^2 + \left(\sigma_2^* - \sigma_3^*\right)^2 + \left(\sigma_3^* - \sigma_1^*\right)^2}. \quad (7)$$

Note that here the σ_1^*, σ_2^*, and σ_3^* are the effective stresses. Also, the strength of the CA mortar elements represented by the nominal stress σ can be obtained with the help of eqs. (1) and (6) .

Substituting eq. (7) into eq. (6) leads to

$$\sigma_i = E\varepsilon_i \exp\left[-\left(\frac{\frac{1}{\sqrt{2}}\sqrt{(\sigma_1^* - \sigma_2^*)^2 + (\sigma_2^* - \sigma_3^*)^2 + (\sigma_3^* - \sigma_1^*)^2}}{F_0}\right)^m\right] + \mu(\sigma_j + \sigma_k). \quad (8)$$

2.3 Determination of parameters of the model

Clearly, there are four unknown parameters included in eq. (6): E, u, F_0, and m. The material parameters E, and u can be obtained through experimental data processing. The physical parameters F_0, and m can be determined by the following approach. Specifically, evaluating the logarithm of both sides of eq. (6) yields

Figure 2 (Color online) Failure model of the CA mortar layer.

$$\ln\left[\sigma_i - \mu\left(\sigma_j + \sigma_k\right)\right] = \ln E\varepsilon_i - \left(\frac{F^*}{F_0}\right)^m. \quad (9)$$

That is

$$-\ln\frac{\sigma_i - \mu\left(\sigma_j + \sigma_k\right)}{E\varepsilon_i} = \left(\frac{F^*}{F_0}\right)^m. \quad (10)$$

Logarithmic evaluations of both sides of eq. (10) lead to

$$\ln\left[-\ln\frac{\sigma_i - \mu(\sigma_j + \sigma_k)}{E\varepsilon_i}\right] = \ln\left(\frac{F^*}{F_0}\right)^m = m\ln\frac{F^*}{F_0} = m\ln F^* - m\ln F_0. \quad (11)$$

Setting

$$y = \ln\left[-\ln\frac{\sigma_i - \mu\left(\sigma_j + \sigma_k\right)}{E\varepsilon_i}\right], \quad (12)$$

$$x = \ln F^*, \quad (13)$$

$$n = m\ln F_0, \quad (14)$$

eq. (11) is simplified as

$$y = mx - n, \quad (15)$$

where m and n can be determined through linear fitting of the experimental data and then using eq. (14) yields

$$F_0 = \exp\left(n/m\right). \quad (16)$$

It is well known that the CA mortar material is quite likely to exhibit a rate-dependent behavior when subjected to vehicle dynamic loads with a high loading rate because of its viscoelasticity. The varying loading rate will perhaps result in different dynamic strengths, and induce nonlinearities on the stress-strain response curves. Therefore, attempts should be made for the constitutive laws to be able to account for this important phenomenon. However, its complexity and the need for some sophistication in the numerical models pose challenges in the railway community. To account for the loading rate dependency, a statistical damage constitutive model with the rate sensitivity can be attempted by relating the physical parameters F_0 and m with the strain rates based on the regression of the experimental data. This will be discussed in detail in Section 4.1

3 Dynamic model of coupled vehicle-slab track system

3.1 Vehicle model

Figure 3 shows the vertically coupled dynamic model of a

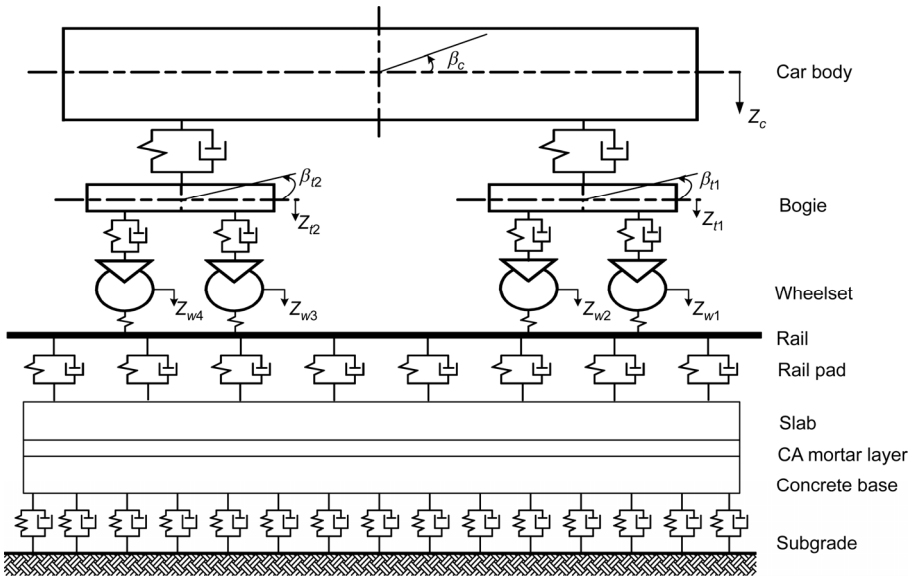

Figure 3 Coupled dynamic model of a vehicle and the CRTS I slab track.

vehicle and the CRTS I slab track which is used to investigate the damage evolution and the dynamic response of the CA mortar layer when the vehicle moves along the slab track. The vehicle is considered as a rigid multi-body model in which the car body is supported on two double-axle bogies with the primary and secondary suspension systems. The primary suspensions, connecting the wheels and the bogie frames, are represented by the spring-damper elements. The secondary suspensions, connecting the bogie frames and the car body, are also modeled as the spring-damper elements. The car body, the bogie, and the wheel are coupled through the suspension elements, as shown in Figure 3. The car body and the two bogies each undergo vertical displacement and pitch rotation, but only the vertical displacement is considered in the four wheels. As a result, the total degrees of freedom of the vehicle are 10. Based on the system of coordinates moving along the track at a constant speed of the vehicle, the equations of the vehicle subsystem can be readily cast in the form of second-order differential equations in the time domain. That is

$$\boldsymbol{M}_V \boldsymbol{A}_V + \boldsymbol{C}_V(\boldsymbol{V}_V)\boldsymbol{V}_V + \boldsymbol{K}_V(\boldsymbol{X}_V)\boldsymbol{X}_V = \boldsymbol{F}_V(\boldsymbol{X}_V, \boldsymbol{X}_T), \quad (17)$$

where $\boldsymbol{M}_V$ is the mass matrix of the vehicle; $\boldsymbol{C}_V$ and $\boldsymbol{K}_V$ are the damping and the stiffness matrices; $\boldsymbol{X}_V$, $\boldsymbol{V}_V$, and $\boldsymbol{A}_V$ are the vectors of displacements, the velocities, and the accelerations of the vehicle subsystem, respectively; $\boldsymbol{X}_T$ is the displacement vector of the track subsystem; and $\boldsymbol{F}_V(\boldsymbol{X}_V, \boldsymbol{X}_T)$ is the system load vector representing the nonlinear wheel/rail contact forces which is a function of the motions $\boldsymbol{X}_V$, of the vehicle and $\boldsymbol{X}_T$ of the track. Detailed descriptions of the equations of the vehicle–track coupled dynamic system can be found in refs. [23,24]

As seen in Figure 3, the vehicle and the slab track are coupled by the interaction force between the rail and the wheel. According to the nonlinear Hertzian theory, the wheel-rail contact force is given by the equation

$$P_j = \begin{cases} \left\{ \frac{1}{G}\left[Z_{wj} - Z_r - Z_0 \right] \right\}^{3/2}, & \text{if } \left(Z_{wj} - Z_r - Z_0 \right) > 0, \\ 0, & \text{else,} \end{cases} \quad (18)$$

where Z_{wj} is the vertical displacement of the jth wheel at time t; Z_r is the vertical rail displacement at the jth wheel position; and Z_0 is the irregularities at the wheel-rail interface.

3.2 Slab track model involving the presented model for the CA mortar

To evaluate the damage evolution and the dynamic performance of the CA mortar layer under vehicle dynamic load, a three-dimensional FE model of the CRTS I slab track system involving the statistical damage constitutive model for the CA mortar layer is built based on the commercial software ABAQUS, as shown in Figure 4. Because of the symmetry of the slab track, and the requirement to improve the computational effort in the present work, half model of the slab track is created: Only a single rail, half of the slab, the CA mortar layer, the concrete slab, and the subgrade are considered, and symmetrical boundary conditions are prescribed on symmetry plane. The slab track system is represented by 2846 solid elements and 5268 degrees of freedom.

In this model, the rail is modeled using the Euler-Bernoulli beam element, with six degrees of freedom (three translations and three rotations) at every node. Hinged boundaries are adopted for the rails to prevent free body motions. The spring-damper elements are employed to represent rail pads at each node. The nodes of these spring-damper elements can move in the vertical and lateral directions with

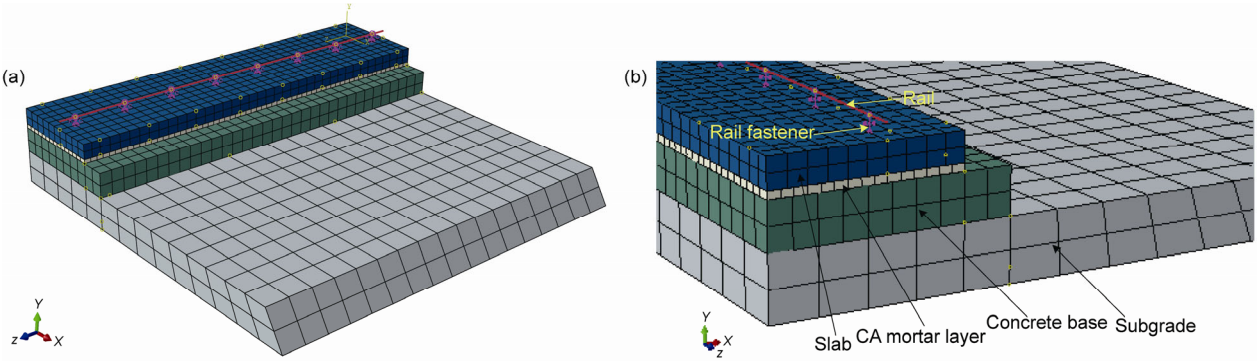

Figure 4 (Color online) Finite element model. (a) The entire finite element mesh; (b) end view of the FE model.

corresponding stiffness and damping. Linear hexahedral elements are applied for the substructure of the slab track, consisting of the slab, the CA mortar layer, the concrete slab, and the subgrade. All the displacements of the nodes at the bottom of the slab track are restricted, and all the nodes at the two ends are subjected to symmetry constraints.

Also, the statistical damage constitutive model for the CA mortar layer is implemented into the FE model as a user-defined material subroutine, whereas the other components are assumed to behave purely elastically. To achieve more accurate results, a relatively fine mesh is used for the CA mortar layer where the material volume undergoes the nonlinear process because of the damage. Note that the inclusion of the strain rate dependence in the physical parameters m and F_0 is considered here, whereas a constant value for the elastic modulus is chosen because of the unsolvable nonlinearities caused by the fluctuated elastic modulus. In the nonlinear calculation, the incremental form of the constitutive law is employed for updating the consistent tangent stiffness matrix in every load increment. That is

$$\frac{\partial \boldsymbol{\sigma}}{\partial \boldsymbol{\varepsilon}} = \boldsymbol{H}' + \left(\frac{\partial \boldsymbol{H}'}{\partial \boldsymbol{\varepsilon}} : \boldsymbol{\varepsilon}\right)\frac{\partial F^*}{\partial \boldsymbol{\sigma}}\frac{\partial \boldsymbol{\sigma}}{\partial \boldsymbol{\varepsilon}} + \left(\frac{\partial \boldsymbol{H}'}{\partial F_0} : \boldsymbol{\varepsilon}\right)\frac{\partial F_0}{\partial \boldsymbol{\varepsilon}} + \left(\frac{\partial \boldsymbol{H}'}{\partial m} : \boldsymbol{\varepsilon}\right)\frac{\partial m}{\partial \boldsymbol{\varepsilon}}, \tag{19}$$

where $\boldsymbol{H}'$ is the elastic stiffness matrix of the damaged CA mortar layer.

Owing to the strain-driven formulation of the proposed constitutive model, its code implementation is quite straightforward, according to the closed-form sequence of operations as indicated in Figure 5.

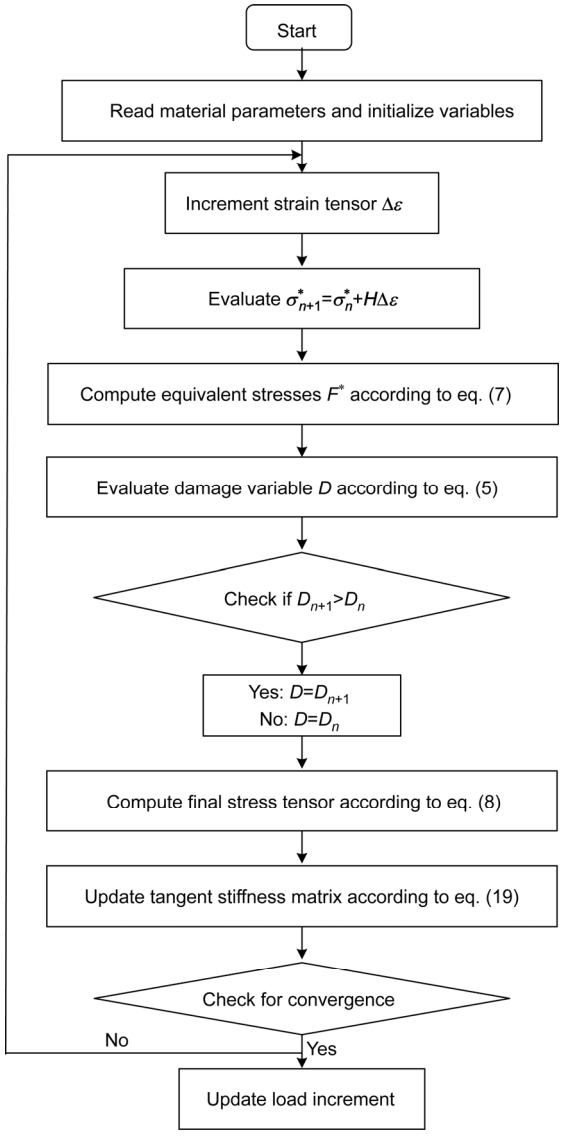

Figure 5 Flow chart of the user material subroutine for the CA mortar layer.

4 Results and discussion

4.1 Experimental validation of the model

To test the validity of the preceding statistical damage constitutive model, the uniaxial compression tests of the CA mortar are conducted as a special case of the complicated stress conditions. Specimens of the CA mortar are made into cylinders with Φ50×50 mm, which satisfy all the physical performance indexes according to the technical requirements of the CA mortar of the CRTS I slab track. The uniaxial

tests are performed on the CSS8810-100kN electronic universal testing machine with the strain controlled loading mode. To study the influence of the strain rates on the dynamic strength and the softening behavior on the stress-stain response curves, five different strain rates, θ(3.3×10^{-6}, 1.7×10^{-4}, 1.7×10^{-3}, 6.6×10^{-3}, and 1.7×10^{-2} s^{-1}), are investigated in the experiments.

Figure 6 shows the stress-strain curves of the CA mortar specimen under the test loadings with the selected strain rates. As the strain rate increases from low to high, the compressive strengths of the CA mortar specimen obtained here are 1.31, 2.03, 3.18, 4.17, and 5.00 MPa, respectively. Their elastic moduli are 193, 299, 477, 488, and 451 MPa, respectively.

Figure 6 shows that before the peak stress, the transition from the elastic strain to the viscous strain is limited at higher strain rates, and therefore, the stored energy is dominated by the elastic stain energy. This also leads to a decrease of the nonlinearity on the stress-stain response curves. Meanwhile, the compressive strengths and the elastic modulus under the higher strain rates are greater than that under the lower rates. This is mainly because at a high strain rate the growth of internal visible cracks is retarded and the energy dissipation is mainly released by the nucleation of microcracks. Thus the dissipated strain energy is much lesser. However, after the peak stress, the rate of energy dissipation under the higher strain rates is greater compared with that under the lower strain rates, representing a reduced strain hardening of the CA mortar in the macroscopic behavior. Such a phenomenon can be attributed to the fact that with the higher strain rates, larger strain energy is dissipated by the much micro-cracks generated before the peak stress.

By substituting the experimental data into eq. (6) and by virtue of eqs. (9)–(16), the parameters of the presented constitutive model can be obtained as shown in Table 1. The fitting stress-stain curves are shown in Figure 7. As can be seen, fitting results of the model for the CA mortar material highlight good agreement quantitatively and qualitatively

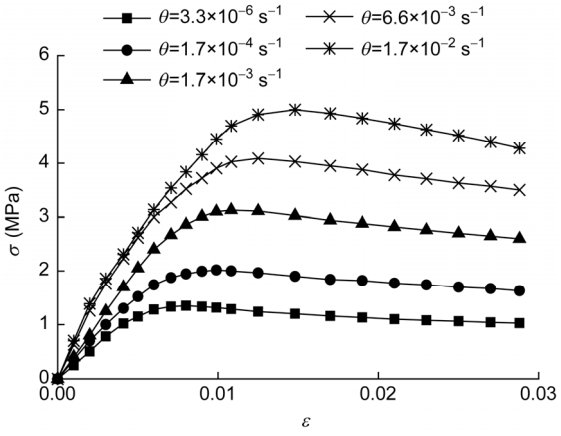

Figure 6 Stress-strain curves of the CA mortar specimens.

Table 1 Parameters fitting results of the constitutive model

Strain rate θ (s^{-1})	E (MPa)	m	F_0	Correlation coefficient
3.3×10^{-6}	193	1.2169	3.790750	0.9452
1.7×10^{-4}	299	1.4101	4.636750	0.9546
1.7×10^{-3}	477	1.4590	8.711980	0.9812
6.6×10^{-3}	488	1.8787	10.61787	0.9803
1.7×10^{-2}	451	2.2397	11.38240	0.9762

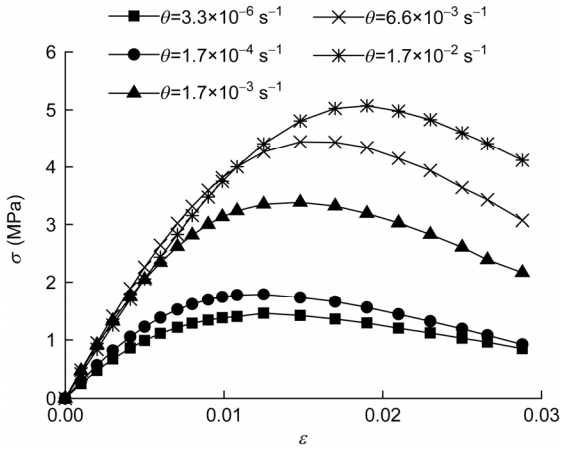

Figure 7 Stress-strain curves of the CA mortar specimens using the presented constitutive model.

compared with the experimental data. Note that an increase in the strain rates result in an increase in the brittleness of the CA mortar, which is manifested by a large drop in the stress after the peak value.

4.2 Inclusion of the strain rate dependency in the model

As can be seen from the above uniaxial tests, increasing the strain rate will induce an increase of the dynamic strength and a reduction in the ductility of the CA mortar material. Also, the physical parameters m and F_0 included in Table 1 show increased tendency with increasing strain rate. To account for the strain rate dependence, the statistical damage constitutive model can be improved by relating the physical parameters m and F_0 with the strain rates. Figure 8 displays the relationship between the parameters m, F_0, E, and the strain rate θ. The related regression functions are described as follows:

$$m = 55.419\theta + 1.3585, \quad R=0.9630, \tag{20}$$

$$F_0 = 20.061\theta^{0.1405}, \quad R=0.9591, \tag{21}$$

$$E = 789.87\theta^{0.1083}, \quad R=0.9462. \tag{22}$$

Upon substituting eqs. (20)–(22) into eq. (6), the stress-strain curves calculated by the modified constitutive model of the CA mortar involving the strain rate dependency can

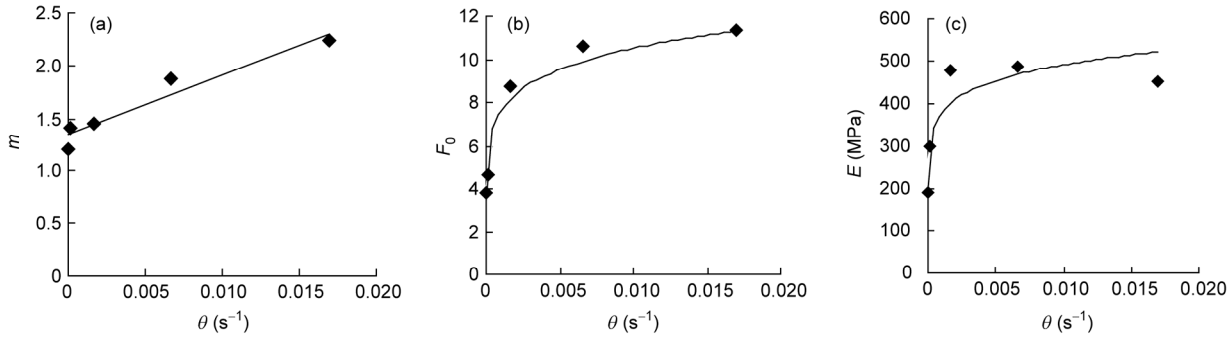

Figure 8 Relation between model parameters and strain rates. Relation between (a) m and θ, (b) F_0 and θ, and (c) E and θ.

be obtained. They are plotted in Figure 9, together with the experimental results. Obviously, the agreement appears to be quite close to all the correlation coefficients greater than 0.9781. Note that as the strain rate increases, the residual strength calculated by the presented model agrees better with the experimental data, revealing that the devised model can describe the transformation from ductility to brittleness with an increase of the strain rate.

It can be concluded from Figure 9 that the CA mortar material has a strong rate sensitivity, which not only affects its dynamic strengths, but also has a great influence on its residual strength and ductility. Also, the mechanism of how the strain rate affects the mechanical properties of the CA mortar can be realized by analyzing the damage characteristics. By applying eq. (5), the damage evolutions as a function of the strain under the uniaxial compression tests is captured in Figure 10. It can be seen that the induced damage increases as the strain increases. With the increasing strain rate, the rate of the damage development decreases, indicating that a larger deformation is required for the CA mortar specimen with a higher strain rate to induce the same damage compared with that with the lower strain rate. Also it can be observed that an increase of the strain rate causes a decrease of the final damage and the damage at the peak strain (the strain at which the peak stress is attained). This shows an increase in the residual strength and the peak stress as the strain rate increases.

In the Sections 4.3 and 4.4, the damage evolution and the dynamic response of the CA mortar layer of the CRTS I slab track exposed to excitations of random track irregularities will be analyzed. Figure 11 presents a sample of the vertical track irregularities generated by means of a time-frequency transformation technique [25,26]. This random track irregularity characterized by the wavelengths from 2 m

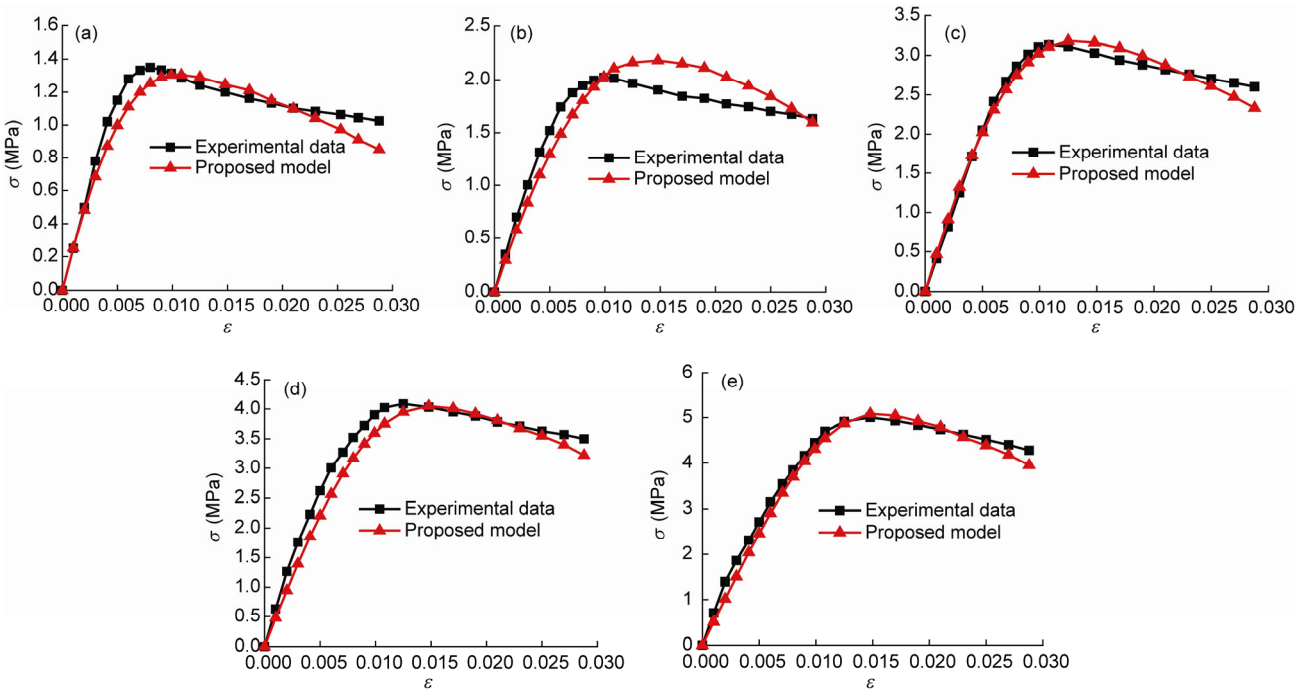

Figure 9 (Color online) Comparison of the stress-strain curves obtained by the constitutive model and experiments: (a) θ=3.3×10^{-6} s^{-1}, (b) θ=1.7×10^{-4} s^{-1}, (c) θ=1.7×10^{-3} s^{-1}, (d) θ=6.6×10^{-3} s^{-1}, (e) θ=1.7×10^{-2} s^{-1}.

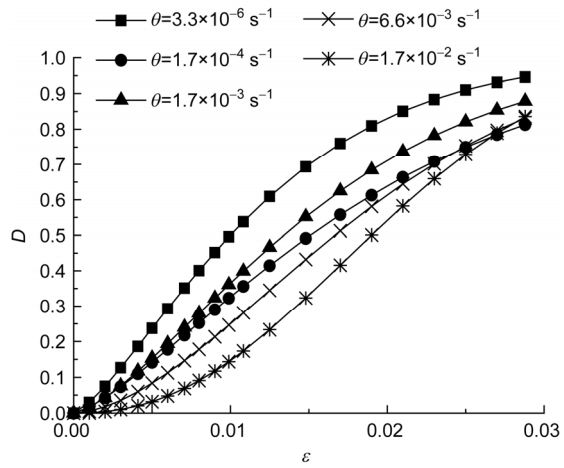

Figure 10 Effect of strain rates on the damage variable.

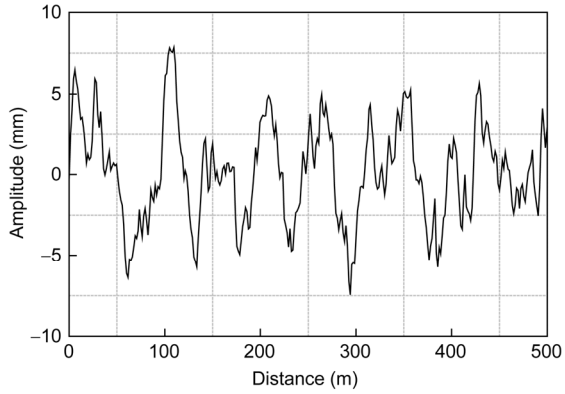

Figure 11 Sample of vertical track irregularity.

to 120 m is adopted as the excitation to the slab track system. The parameters of a passenger vehicle and the CRTS I slab track system adopted in this work are listed in Tables 2 and 3.

Table 2 Vehicle parameters

Parameters	Values	Units
Car body mass	26100	kg
Car body pitch moment of inertia	1.2789×10^{6}	kg m^2
Bogie mass	2600	kg
Bogie pitch moment of inertia	1424	kg m^2
Wheelset mass	2100	kg
Primary suspension stiffness	1.176×10^{6}	N/m
Primary suspension damping	1.8914×10^{5}	N s/m
Secondary suspension stiffness	2×10^{4}	N/m
Secondary suspension damping	6×10^{4}	N s/m
Distance between two bogie centers	17	m
Distance between two axles of same bogie	2.5	m
Wheel rolling radius	0.43	m

Table 3 CRTS I slab track parameters

Parameters	Values	Units
Rail mass per unit length	60.64	kg
Area moment of the rail cross section	3.217×10^{-5}	m^4
Rail elastic modulus	2.059×10^{11}	Pa
Slab length	4.962	m
Slab width	2.4	m
Slab height	0.19	m
Slab elastic modulus	3.5×10^{10}	Pa
CAM layer length	4.962	m
CAM layer width	2.4	m
CAM layer height	0.05	m
CAM layer elastic modulus	2×10^{8}	Pa
Concrete base width	3	m
Concrete base height	0.3	m
Concrete base elastic modulus	5×10^{9}	Pa
Subgrade elastic modulus	1.9×10^{8}	Pa

4.3 Damage evolution of the CA mortar layer under vehicle dynamic load

Figure 12 shows the time histories of the excited wheel-rail forces when the passenger vehicle travels at a speed of 200 km/h through the slab track with the irregularity described above. Also shown in Figure 13 is the typical time history of the rail-supporting force. It can be clearly seen that there are four peak values of about 18 kN because of the vehicle passage through the slab track. For brevity, the other rail-supporting forces are not listed below.

To investigate how the damage of the CA mortar layer evolves under the obtained vehicle dynamic load, the damage developments of the CA mortar layer with various initial damage, which represents various service stages are next analyzed. This is done by conducting nonlinear dynamic analysis based on the ABAQUS dynamic implicit code implemented with the presented constitutive model. As shown in Figure 14, the CA mortar damage starts occurring when the front bogie is passing, and it further evolves as the rear bogie passes. Evidently, with the increasing initial damage, the development rate of the CA mortar damage increases significantly. The degree of the damage development for the CA mortar layer predicted here is consistent with the damage observed in the uniaxial compression tests. It can be seen from Figure 14 that the induced maximum damage of the CA mortar layer with the initial damage of 0.75 is around 0.14, which is about 3.5 times as large as that with the initial damage of zero. Such phenomena are most likely because much more internal micro-cracks are accumulated for the CA mortar layer with a larger initial damage, and thus weaken its dynamic strength. It is clearly shown in Figure 15 that under the vehicle dynamic load the CA mortar damage grows sharply at the relatively low strain rates,

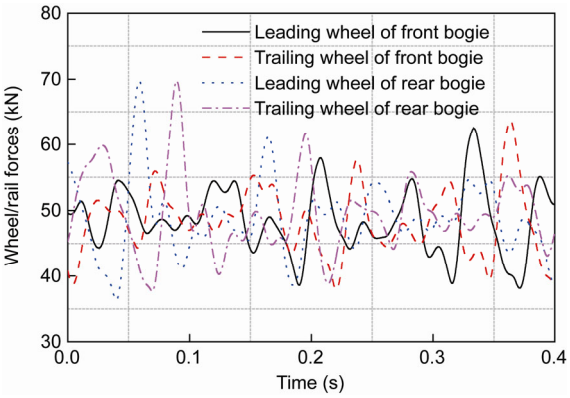

Figure 12 (Color online) Time histories of the excited wheel/rail forces.

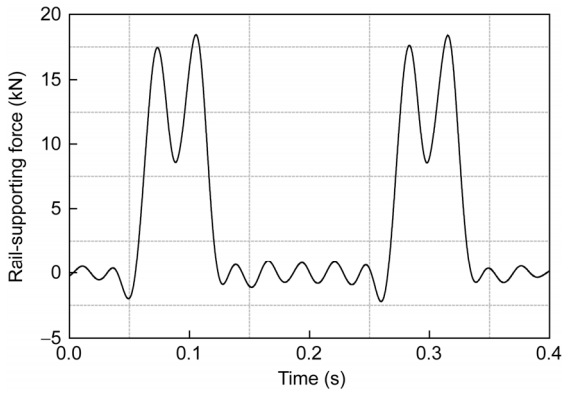

Figure 13 Time histories of the rail-supporting forces.

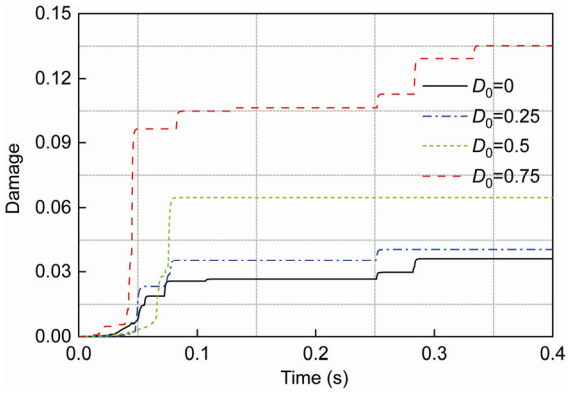

Figure 14 (Color online) Damage evolution of the CA mortar layer with various initial damage levels during the vehicle passing.

whereas it keeps constant at the high strain rates. This is because the higher strain rates lead to the higher dynamic strengths. The results of the strain rate evolution given in Figure 16 clearly show an increase in the strain rates with the initial damage. The maximum strain rate for the CA mortar layer with the initial damage of 0.75 is found to be 0.05 s^{-1}, which is approximately five times that with the initial damage of zero. Therefore, it can be argued that a higher strain rate at a larger damage state will, to some extent, preclude the development of the CA mortar damage,

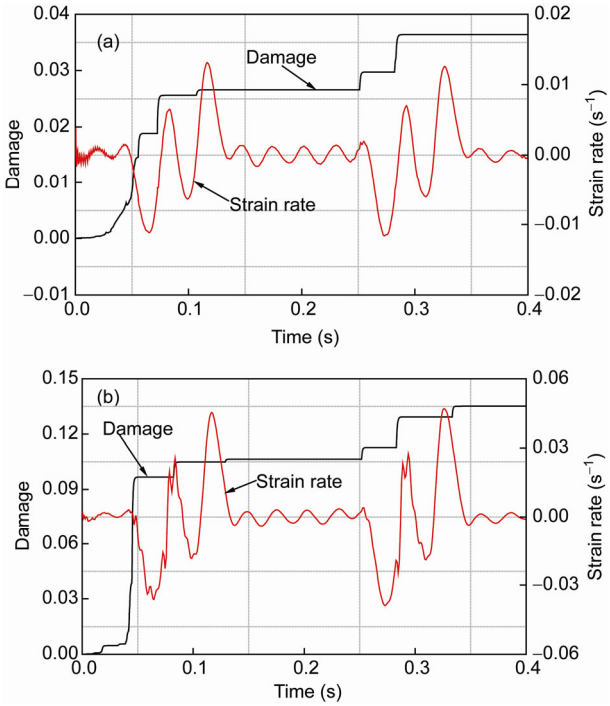

Figure 15 (Color online) Effect of strain rates variation on the damage evolution of the CA mortar layer under vehicle dynamic load: (a) The case for the initial damage D_0=0, (b) the case for the initial damage D_0=0.75.

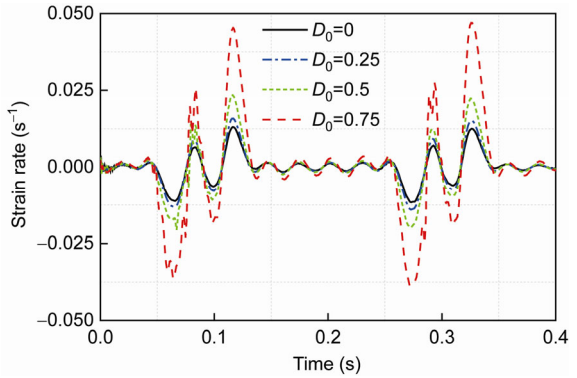

Figure 16 (Color online) Strain rate evolution of the CA mortar layer with various initial damage during the vehicle passing.

which is beneficial for the structural safety and the running stability of high-speed trains.

4.4 Dynamic response of the CA mortar layer under vehicle dynamic load

Figures 17 and 18 show the obtained dynamic response of the CA mortar layer with various initial damages. This is in terms of the dynamic compressive stress and strain, when the vehicle passes with the previous train's speed. As the initial damage increases, a notable reduction of the compressive stress is seen in Figure 17, whereas a substantial increase of the compressive strain is observed in Figure 18. At this state, it may lead to the formation of track dynamic

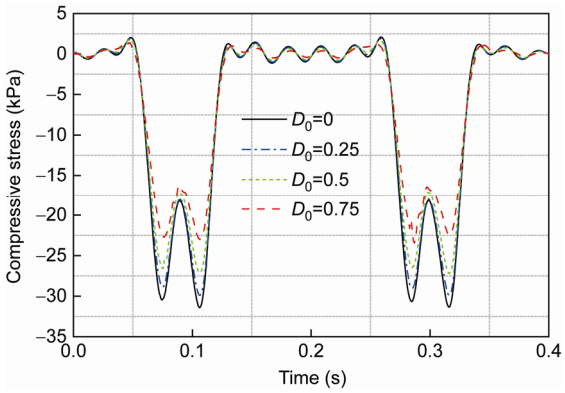

Figure 17 (Color online) Dynamic compressive stress induced by the vehicle passage.

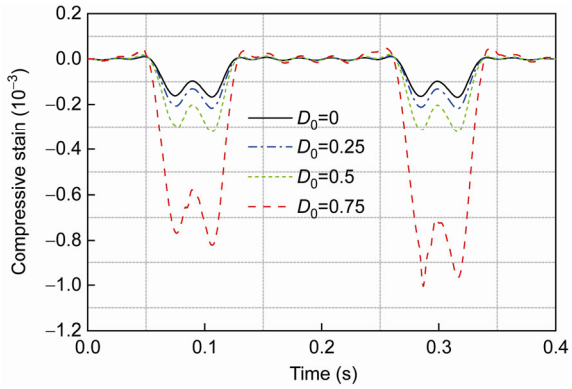

Figure 18 (Color online) Dynamic compressive strain induced by the vehicle passage.

irregularities. Thus, it will most likely alter the running behavior of high-speed trains. For the CA mortar layer with the initial damage of 0.75, the maximum value of the dynamic compressive stress is 23 kPa, which is smaller than that with the initial damage of zero by about 35%. Also, the maximum value of the dynamic compressive strain is 0.001, which is about 6.25 times as large as the result for the initial damage of zero. Such a phenomenon represents well the nonlinear behavior of the strain softening of the CA mortar layer because of the increasing damage. This property is in accordance with that observed in the uniaxial compression experiments. It is worth pointing out that for the CA mortar layer with the initial damage of 0.75, larger compressive strain caused by the rear bogie can be identified in Figure 18, compared with that induced by the front bogie. This is mainly because of the significant damage development of 0.14 in this case.

For completeness, the evolution of contour plots of the compressive stress are shown in Figure 19 when the front bogie is inside the computational domain and its excitation is initiated. Considering that the evolution of dynamic response is essentially because of the damage development of

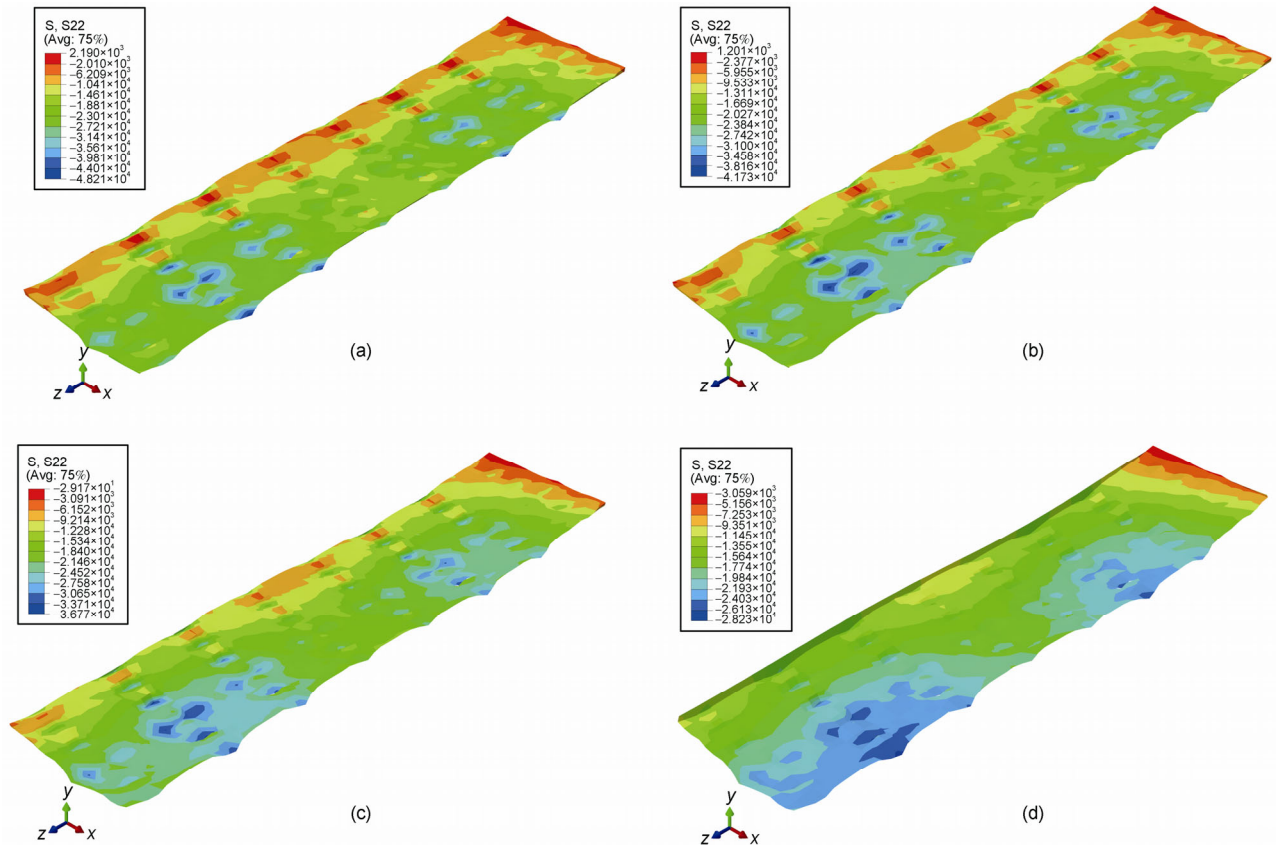

Figure 19 (Color online) Stress contours of the CA mortar layer when the front bogie is inside the computational domain: (a) The case for the initial damage D_0=0, (b) D_0=0.25, (c) D_0=0.5, and (d) D_0=0.75 (deformation scale factor is 5000).

the CA mortar layer, it is understandable that decreasing compressive stress contours can be seen in Figure 19 as the damage increases. It should be noted that the simulation results may not be able to accurately reflect the damage evolution and dynamic performance of actual CA mortar layers in service, because of the fact that the damage can be induced by other complicated environmental loads.

5 Conclusions

In this paper a statistical damage constitutive model for the CA mortar material accounting for the strain rate dependency has been proposed and validated by experiments. This model is based on the Mises strength criterion, which obeys the Weibull distribution. As a user-defined material subroutine, the devised model for the CA mortar layer has been implemented into a three-dimensional finite element (FE) model of the CRTS I slab track. Based on the vehicle-track coupled dynamic theory, the evolution of the damage and of the dynamic response of the CA mortar layer with various initial damage has been investigated under vehicle dynamic load. The findings can be summarized as follows.

1) The proposed constitutive model with only a few parameters is quite suitable and accurate for the damage evolution analysis of the CA mortar layer of the slab track subjected to vehicle dynamic load.

2) The model for the CA mortar layer can well reproduce the transition from the ductility to the brittleness with the increasing strain rate. Its implementation into the FE model of the slab track for the dynamic analysis affords capturing the nonlinear response of the strain softening because of the increasing damage.

3) The CA mortar layer of the slab track exhibits a strong rate sensitivity, which not only affects its dynamic strength, but also its damage evolution. An increase of the strain rate will induce a reduction in the damage development, and an increase of the dynamic strength.

4) The induced damage, the strain rate, and the dynamic compressive strain increase significantly with an increase in the initial damage, whereas the dynamic compressive stress shows a notable decrease with the increasing damage.

This work was supported by the National Basic Research Program of China ("973" Project) (Grant Nos. 2013CB036202, 2013CB036200), the National Natural Science Foundation of China (Grant No. 51008254), the Funds from the Key Laboratory for Precision & Non-traditional Machining of the Ministry of Education, Dalian University of Technology (Grant No. JMTZ201002), the Fundamental Research Funds for the Central Universities (Grant No. 2682013CX029), the Funds from the China Scholarship Council, and the 2013 Cultivation Program for the Excellent Doctoral Dissertation of Southwest Jiaotong University.

1 Esveld C. Modern Railway Track. Zaltbommel: MRT-Productions, 2001. 231–274
2 Galvin P, Romero A, Dominguez J. Vibrations induced by hst passage on ballast and non-ballast tracks. Soil Dyn Earthq Eng, 2010, 30: 862–873
3 Lei X, Zhang B. Analysis of dynamic behavior for slab track of high-speed railway based on vehicle and track elements. J Transp Eng-ASCE, 2011, 137: 227–240
4 Deng D H. The research report of 50878209 proposal financially supported by the national science foundation of P R China (in Chinese). Changsha: Central South University, 2012
5 Xie Y J, Zeng X H, Deng D H, et al. Mechanical characteristics of China railway track system (CRTS) I type slab track CA mortar under different strain rates (in Chinese). Chin J Build Mater, 2010, 13: 483–486
6 Zeng X H, Xie Y J, Deng D H, et al. Vibration adsorption and seperation capacities of CA mortar (in Chinese). Chin J Build Mater, 2013, 16: 345–348
7 Zhu S Y, Cai C B. Interface damage and its effect on vibrations of slab track under temperature and vehicle dynamic loads. Int J Nonlinear Mech, 2014, 58: 222–232
8 Liu Y, Zhao G T. Analysis of early gap between layers of CRTS II slab ballastless track structure (in Chinese). China Railway Sci, 2013, 34: 1–7
9 Shao P Y, Li H Y, Wu S L, et al. Measurement and research on temperature warping of CRTS I track slab and crack between track slab and cement asphalt mortar cushion (in Chinese). China Railway Sci, 2013, 34: 18–22
10 Chaboche J L. Continuum damage mechanics. Part I: General concepts. J Appl Mech, 1988, 55: 59–64
11 Simo J C, Ju J W. Strain and stress-based continuum Damage models. Part I: Formulation. Int J Solids Struct, 1987, 23: 821–840
12 Chow C L, Wang J. An anisotropic theory of elasticity for continuum damage mechanics. Int J Fracture, 1987, 33: 2–16
13 Lee J, Fenves G L. Plastic-damage model for cyclic loading of concrete structures. J Eng Mech-ASCE, 1998, 124: 892–900
14 Hansen N R, Schreyer H L. A thermodynamically consistent framework for theories of elastoplasticity coupled with damage. Int J Solids Struct, 1994, 31: 359–389
15 Voyiadjis G Z, Taqieddin Z N, Kattan P I. Anisotropic damage-plasticity model for concrete. Int J Plasticity, 2008, 24: 1946–1965
16 Comi C, Perego U. Fracture energy based bi-dissipative damage model for concrete. Int J Solids Struct, 2001, 38: 6427–6454
17 Faria R, Oliver J, Cervera M. Modeling material failure in concrete structures. J Struct Eng-ASCE, 2004, 130: 1997–2005
18 Li S Y, Lai Y M, Zhang S J, et al. An improved statistical damage constitutive model for warm frozen clay based on Mohr-Coulomb criterion. Cold Reg Sci Tech, 2009, 57: 154–159
19 Massoudi M, Mehrabadi M M. A continuum model for granular materials: Considering dilatancy and the Mohr-Coulomb criterion. Acta Mech, 2001, 152: 121–138
20 Bousshine L, Chaaba A, Saxce G D. Softening in stress–strain curve for Drucker-Prager non-associated plasticity. Int J Plasticity, 2001, 17: 21–46
21 Hjiaj M, Fortin J, de Saxcé G. A complete stress update algorithm for the non-associated Drucker-Prager model including treatment of the apex. Int J Eng Sci, 2003, 41: 1109–1143
22 Sinka I C, Cunningham J C, Zavaliangos A. The effect of wall friction in the compaction of pharmaceutical tablets with curved faces: A validation study of the Drucker-Prager cap model. Powder Technol, 2003, 133: 33–43
23 Zhai W. Vehicle-track Coupled Dynamics (in Chinese). Beijing: Science Press, 2007. 20–38
24 Zhai W, Wang K, Cai C. Fundamentals of vehicle-track coupled dynamics. Veh Syst Dyn, 2009, 47: 1349–1376
25 Chen G, Zhai W. Numerical simulation of the stochastic process of railway track irregularities (in Chinese). J Southwest Jiaotong Univ, 1999, 34: 138–142
26 Spanos P D, Zeldin B A. Monte Carlo treatment of random fields: A broad perspective. Appl Mech Rev, 1998, 51: 219–236